Study of Ho-doped Bi2Te3 topological insulator thin films

S. E. Harrison, L. J. Collins-McIntyre, S. L. Zhang, A. A. Baker, A. I. Figueroa, A. J. Kellock, A. Pushp, Y. L. Chen , S. S. P. Parkin, J. S. Harris, G. van der Laan, and T. Hesjedal

Citation: Applied Physics Letters **107**, 182406 (2015); doi: 10.1063/1.4935235
View online: http://dx.doi.org/10.1063/1.4935235
View Table of Contents: http://scitation.aip.org/content/aip/journal/apl/107/18?ver=pdfcov
Published by the AIP Publishing

Study of Ho-doped Bi_2Te_3 topological insulator thin films

S. E. Harrison,[1,2] L. J. Collins-McIntyre,[1] S. L. Zhang,[1] A. A. Baker,[1,3] A. I. Figueroa,[3] A. J. Kellock,[4] A. Pushp,[4] Y. L. Chen,[1] S. S. P. Parkin,[4] J. S. Harris,[2] G. van der Laan,[3] and T. Hesjedal[1,a)]

[1]*Department of Physics, Clarendon Laboratory, University of Oxford, Oxford OX1 3PU, United Kingdom*
[2]*Department of Electrical Engineering, Stanford University, Stanford, California 94305, USA*
[3]*Magnetic Spectroscopy Group, Diamond Light Source, Didcot OX11 0DE, United Kingdom*
[4]*IBM Almaden Research Center, 650 Harry Road, San Jose, California 95120, USA*

(Received 22 September 2015; accepted 25 October 2015; published online 3 November 2015)

Breaking time-reversal symmetry through magnetic doping of topological insulators has been identified as a key strategy for unlocking exotic physical states. Here, we report the growth of Bi_2Te_3 thin films doped with the highest magnetic moment element Ho. Diffraction studies demonstrate high quality films for up to 21% Ho incorporation. Superconducting quantum interference device magnetometry reveals paramagnetism down to 2 K with an effective magnetic moment of $\sim 5\,\mu_B$/Ho. Angle-resolved photoemission spectroscopy shows that the topological surface state remains intact with Ho doping, consistent with the material's paramagnetic state. The large saturation moment achieved makes these films useful for incorporation into heterostructures, whereby magnetic order can be introduced via interfacial coupling. [http://dx.doi.org/10.1063/1.4935235]

Topological insulators (TIs) have gained strong interest as a new class of materials with fascinating yet exotic physics.[1,2] They host a gapless time-reversal symmetry (TRS) protected topological surface state (TSS) that exhibits a Dirac-cone like dispersion. Breaking the TRS in TIs through magnetic doping can result in a gap forming at the Dirac-point in the TSS.[3,4] This altered bandstructure may host a variety of interesting physical phenomena, such as the quantum anomalous Hall effect (QAHE).[5] The prediction of novel quantized states arising from the peculiar coupling between magnetic and electric fields[6] make ferromagnetic TIs an intriguing venue for the next generation of electronic and spintronic devices. Potential applications of ferromagnetic TIs include interconnects, memory cells, and other novel electronics.[7–10]

The three-dimensional TIs Bi_2Te_3 and Bi_2Se_3 are the most thoroughly investigated class of TI materials due to their (comparably) large bulk bandgaps of 0.15–0.3 eV and simple, single Dirac-cone, surface states.[11] Ferromagnetic order has been achieved by transition metal doping,[12] e.g., with Fe,[13] Mn,[14–18] and Cr,[19–21] of bulk and thin film samples. A major concern for magnetic TI doping, however, is to avoid the introduction of additional charge carriers in the material. In principle, transition metal dopants such as Cr should enter the host in their 3+ state, substituting for Bi; however, recent x-ray spectroscopy found Cr to be divalent in Bi_2Se_3.[22,23] Doping with most rare earth (RE) ions, on the other hand, has the advantage of substituting Bi^{3+} isoelectronically with RE^{3+}, as well as introducing a large magnetic moment into the system which may lead to increased TRS-breaking effects. The effective magnetic moment of Gd^{3+}, which has the maximum number of 7 unpaired f electrons in the lanthanide series, is $7.94\,\mu_B$. However, even higher effective moments of $10.4\,\mu_B$ and $10.6\,\mu_B$ are found for Dy^{3+} ($4f^9$) and Ho^{3+} ($4f^{10}$), respectively, due to spin-orbit coupling.

Recently, we presented the growth of high quality rhombohedral Gd- and Dy-doped Bi_2Te_3 thin films by molecular beam epitaxy (MBE) with high RE concentrations (up to 40% of the Bi sites), exceeding reported bulk solubility limits.[24–27] In this letter, we present the MBE growth and a structural, magnetic, and electronic properties study of $(Ho_xBi_{1-x})_2Te_3$ topological insulator thin films, which aims to expand on the current understanding of the effects of RE doping in TIs.

$(Ho_xBi_{1-x})_2Te_3$ thin films $(0 \le x \le 0.21)$ were grown on c-plane sapphire substrates using MBE. Prior to growth, cleaned 2 in.-diameter substrates were introduced into the main growth chamber with a base pressure of $\sim 5 \times 10^{-11}$ Torr. The substrate temperature, determined by a thermocouple, was ramped up to 450 °C for ~10 min before ramping down to the starting growth temperature. Thin film deposition was carried out by co-evaporation of high purity Bi (6 N), Te (6 N), and Ho (4 N) from standard Knudsen effusion cells. The Ho concentration, x, was controlled by varying the Ho effusion cell temperature ($T_{Ho} = 840$–900 °C), while the Bi and Te cell temperatures were held constant (458 °C and 235 °C, respectively), which resulted in a nominal Te:Bi ratio of ~15. The Ho, Bi, and Te cell fluxes were calibrated using an ion gauge beam flux monitor.

A two-temperature-step process,[28] similar to the recipe described in Refs. 26, 27 and 29, was used for growth of the $(Ho_xBi_{1-x})_2Te_3$ thin films. During the first growth step, a low temperature nucleation layer was deposited for 33 min at 250 °C. Film growth was then paused while the substrate temperature was ramped up to 300 °C under Te flux at a rate of 5 °C min^{-1}. At 300 °C, the sample was annealed for

a)Author to whom correspondence should be addressed. Electronic mail: Thorsten.Hesjedal@physics.ox.ac.uk

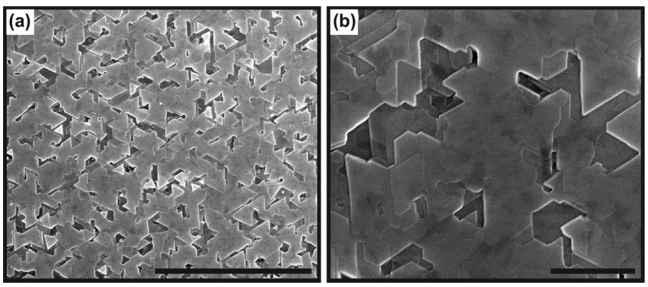

FIG. 1. ((a) and (b)) SEM images for an $x = 0.14$ film. The scale bar in (b) represents 5 μm and in (c) 500 nm.

30 min before growth continued at 300 °C for another 33 min. After growth was terminated, samples were allowed to cool to room temperature. *In-situ* reflection high energy electron diffraction was used to provide real-time feedback about the surface morphology, and the results are shown in the supplementary material.[30] The surface morphology of the Ho-doped films was also further investigated by *ex-situ* measurements using scanning electron microscopy (SEM). Typical examples of large- and small-area scans, showing the characteristic triangular domain structure known from undoped and doped Bi_2Te_3 thin films,[26] are shown in Figs. 1(a) and 1(b), respectively, for a film grown with $T_{Ho} = 840$ °C.

Compositional analysis was carried out using a combination of Rutherford backscattering spectroscopy (RBS) with 2.3 MeV He ions and particle induced x-ray emission (PIXE) with 1 MeV H ions. For materials composed of more than one heavy element peak overlap in RBS can lead to uncertainty in the composition determination. For our studies, the peak overlap between the constituent heavy elements was resolved using PIXE.

The combined RBS/PIXE results are summarized in Table I. Note that a small Se concentration was detected as well, which resulted from a Se background contamination of the MBE growth chamber. In all cases, the Se and Te concentrations were found to add up to ~60 at. % (atomic-%) within error, which suggests that Se is replacing Te in the lattice. In addition, analysis of the cation (Ho+Bi) to anion (Te+Se) ratios shows a relationship of ~2:3, within the specified error margin, which is indicative of Ho being mostly substitutional on Bi sites for the doping series.[24]

X-ray diffraction (XRD) measurements were performed to investigate the effects of Ho incorporation on the structural properties of the Bi_2Te_3 host. Figure 2(a) shows symmetric 2θ–ω scans obtained using Cu Kα_1 emission and a triple-axis detector in grazing-incidence configuration. Only substrate

TABLE I. Composition and thickness t determined by RBS and PIXE measurements for thin films grown at the indicated Ho cell temperatures, T_{Ho}. The error for the elemental compositions is 0.5 at. % for Se and all elements for the nominally undoped film, and 2 at. % otherwise.

T_{Ho} (°C)	x_{Ho}	Ho (at. %)	Bi (at. %)	Te (at. %)	Se (at. %)	t (Å)
…	0	0.0	39.2	59.7	1.1	721 ± 50
840	0.14	5.5	35.8	56.4	2.3	800 ± 100
865	0.21	8.4	33.4	55.3	2.9	941 ± 100

and film peaks corresponding to the relative positions of the Bi_2Te_3 (0 0 l) family of diffraction peaks were observed, as expected for c-axis oriented $(Ho_xBi_{1-x})_2Te_3$ thin films in a rhombohedral crystalline structure. In addition, the absence of additional peaks in the spectra indicates that no secondary phases were detected up to $x = 0.21$.

Careful analysis of the Bragg peaks in Fig. 2(a) reveals that the peaks shift toward lower diffraction angles and experience broadening as a function of doping concentration, which are consistent with observations for other MBE-grown RE-doped Bi_2Te_3 thin films.[24,26,27] The appearance of these effects is indicative of an increased out-of-plane lattice constant and degradation in overall crystalline quality with increasing Ho doping. The expansion of the out-of-plane lattice parameter c, determined from the 2θ values of the (0 0 l) peaks for 5°–65° using a nonlinear least-square cell-refinement program,[31] is plotted in Fig. 2(b) (left axis). The increase of ~0.3 Å at $x = 0.21$ is slightly larger than the increase in c for Dy-doped films with similar x.[27]

Evidence of the degradation of crystallinity is further observed in the increase in the full-width at half maximum (FWHM) of the (0 0 6) rocking curves, as shown in Fig. 2(b) (right axis). Films with $x = 0.14$, however, were found to be of relatively high crystalline quality with only an increase of ~0.046° in the (0 0 6) FWHM when compared to the undoped film. In addition, when compared to other magnetically doped TI films with similar doping concentrations, the FWHM of the (0 0 6) rocking curve for the $x = 0.14$ sample was ~7.50× smaller and ~0.57× larger than the values obtained for Cr-doped[21] and Dy-doped films, respectively. Additional rocking curve analysis and 2D asymmetric reciprocal space mappings can be found in the supplementary material.[30]

Bulk magnetization measurements were carried out on the Ho-doped samples using a superconducting quantum interference device (SQUID) magnetometer (7 T Quantum Design MPMS SQUID VSM). Figure 3(a) shows $M(H)$ plots obtained at 2 K for films with $x = 0.14$ and $x = 0.21$ in an

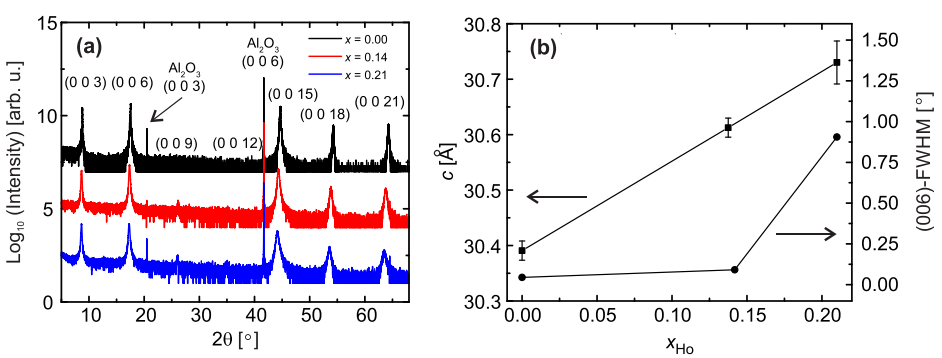

FIG. 2. XRD measurements. (a) 2θ–ω scans obtained on an undoped binary Bi_2Te_3 thin film (black), and $(Ho_xBi_{1-x})_2Te_3$ films with $x = 0.14$ (red) and 0.21 (blue). The (0 0 l) film and substrate peaks are labeled. (b) Left axis: Out-of-plane lattice parameter c obtained from the (0 0 l) reflections. Right axis: FWHM of the (0 0 6) rocking curves.

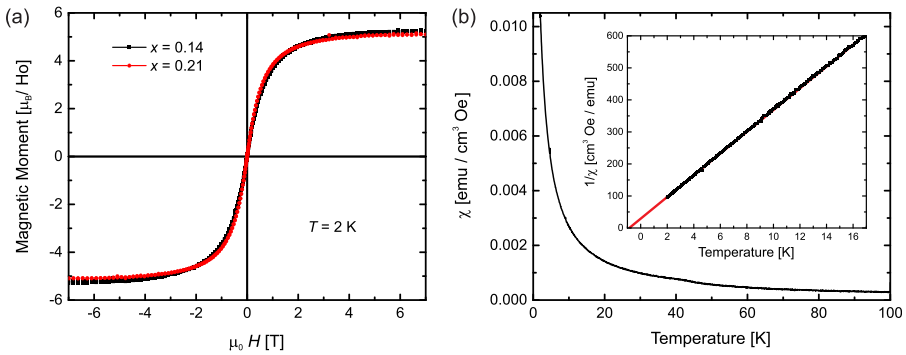

FIG. 3. SQUID magnetometry. (a) $M(H)$ plots obtained at 2 K for $x = 0.14$ and $x = 0.21$ with the field applied in-plane. (b) Plot of the susceptibility, χ, as a function of temperature. Inset: Plot of $1/\chi$ for the $x = 0.14$ sample. The intercept Θ is negative (≈ -0.8 K).

applied magnetic field ranging between ± 7 T. Measurements were performed with the field applied perpendicular to the c-axis, i.e., in-plane. In order to isolate the film signals, the diamagnetic background from the sapphire substrate was removed via high-field linear fitting. The shape of the magnetization curves resembles the Brillouin function, which is indicative of paramagnetic behavior. The magnetic moments per Ho ion [Fig. 3(a)] were obtained using the film volume, determined from the mass of the sample and the RBS/PIXE thickness measurements, and the Ho concentration from the RBS/PIXE data. The saturation moments were found to be (5.20 ± 0.74) μ_B/Ho and (5.08 ± 0.60) μ_B/Ho for $x = 0.14$ and $x = 0.21$, respectively. The stated errors are determined by the uncertainty in the determination of sample volume from the RBS/PIXE data. The moments were found to be fully saturated at $\sim$4 T (at 2 K), and, within the errors, independent of the doping concentration. The observed moments are significantly less than the theoretical free-ion value of $\sim 10.6\,\mu_B$ for Ho^{3+} and may arise from oxidation of the Ho dopants, crystal-field effects, and/or the appearance of antiferromagnetic coupling.[20,32,33]

Magnetization vs. temperature measurements in an applied field of 100 mT, shown in Fig. 3(b) for a film with $x = 0.14$, were also performed. All films in the doping series yielded $M(T)$ plots that exhibited a typical paramagnetic response. A plot of the inverse susceptibility, $1/\chi$, is shown in the inset in Fig. 3(b). In order to highlight deviations from the paramagnetic behavior, the susceptibility was fitted using the Curie-Weiss dependence, $\chi = C/(T - \Theta)$, where C is the material-specific Curie constant and Θ the Weiss temperature. The fit for $x = 0.14$ is shown by the red line in Fig. 3(b) and reveals a negative Weiss temperature $[\Theta = (-0.837 \pm 0.007)$ K], which points towards possible antiferromagnetic ordering at low temperatures. Similar results were also obtained on Ho-doped films with $x = 0.21$.

The element-specific technique of x-ray magnetic circular dichroism (XMCD) is used to probe the local electronic character of the magnetic ground state.[34] X-ray absorption spectra (XAS) at the Ho $M_{4,5}$ edges were measured on beamline I10 (BLADE) at the Diamond Light Source, Oxfordshire, using a 14 T superconducting magnet. XAS measurements were made in total-electron-yield (TEY) mode. The XMCD is obtained from the difference between two XAS spectra recorded with the x-ray helicity vector and applied magnetic field parallel and antiparallel, respectively.[35] The magnetic field is always parallel to the x-ray beam and the samples (with the normal $\|$ c-axis) were measured at both normal and grazing incidence. The XMCD is measured by reversing the polarization of the incident x-rays to avoid having to change the magnetic field of the superconducting magnet.

Unlike the 5*d* and 6*s* electrons in Ho, the 4*f* electrons are not directly involved in the chemical bonding. Therefore, the Ho $M_{4,5}$ spectrum is essentially the same for the metal and alloys, as well as oxides and compounds, apart from small differences in line broadening. Since the additional 4*f* electron is effectively screening the 3*d* hole, the chemical shift in the $M_{4,5}$ spectra is small, so that no chemical information is obtained from the XAS and XMCD spectra. However, the magnitude of the XMCD signal is directly proportional to the 4*f* magnetic moment.[36,37]

Figure 4 shows the Ho M_5 XMCD for the Ho-doped Bi_2Te_3 thin film with $x = 0.14$, measured over a range of temperatures with an out-of-plane applied field of 7 T. The moment is zero at 300 K, and gradually increases for decreasing temperature. An estimation of the Weiss temperature may be obtained from the inverse of the magnetic susceptibility $1/\chi = H/M$ (using the moment obtained from XMCD) as a function of temperature. This shows the typical linear dependency expected for a paramagnetic system.

Angle-resolved photoemission spectroscopy (ARPES) measurements were performed to investigate the electronic structure of the Ho-doped films. ARPES makes direct measurement of the spectral function of the probed material which is, in general, related to its electronic bandstructure. Figure 5 shows the ARPES data obtained at 20 K on an *in-situ* cleaved Ho-doped Bi_2Te_3 thin film with $x = 0.14$.[38] The presence of the topological surface state band (SSB) is resolved in the 3D representation shown in Fig. 5(a). The

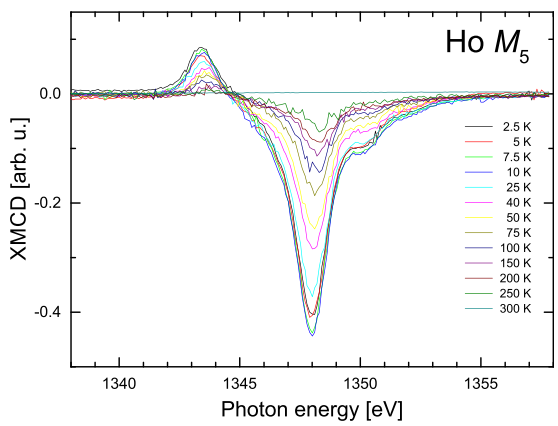

FIG. 4. Temperature-dependent Ho M_5 XMCD measurements of a film with $x = 0.14$ in TEY mode at normal incidence in an applied field of 7 T.

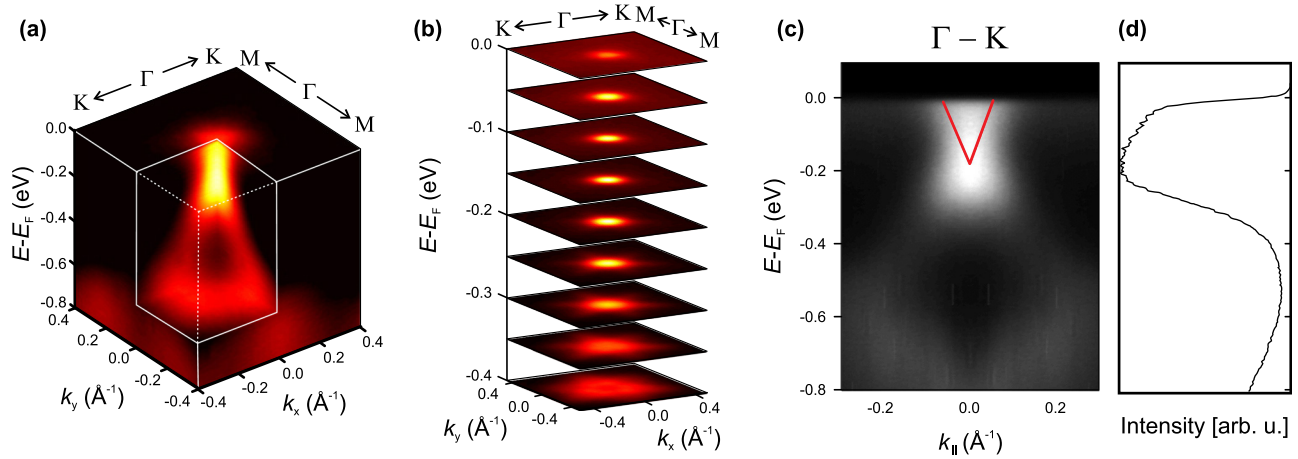

FIG. 5. Bandstructures of an *in-situ* cleaved Ho-doped thin film with $x = 0.14$. (a) 3D illustration showing the band dispersion in the 2D Brillouin zone. (b) Stack of constant energy maps at the binding energies, $E - E_F$. Both the surface state band (SSB) and the bulk valence band (BVB) are resolved. The BVB shows a six-fold symmetry. (c) Cut of the 3D bandstructure along the Γ-K direction, and (d) intensity profile (energy distribution curve) at $k_{\|} = 0$. No intensity suppression is seen in the bandstructure near the Dirac-point.

Fermi velocity obtained along the Γ-K direction was found to be approximately 4.7×10^5 m s^{-1} (2.5 eV Å) which is similar to values reported for undoped single-crystal and thin film Bi_2Te_3 [Refs. 28 and 39] as well as Gd-doped Bi_2Te_3 thin films.[24,38] Stacked constant energy mappings showing the evolution of the SSB and bulk valance band (BVB) for different binding energies are provided in Fig. 5(b). At more negative binding energies, the disappearance of the SSB and the emergence of the hexagram-like BVB are observed and consistent with previous reports on Bi_2Te_3.[39] Note that the bulk conduction band is not visible in the data shown in Fig. 5 due to the relative position of the Fermi level.

Bandstructure data obtained at 50 eV along the Γ-K direction is shown in Fig. 5(c), where the surface state band is indicated in red. The energy distribution curve at $k_{\|} = 0$ is provided in Fig. 5(d). No indication of a magnetic doping-induced gap at the Dirac-point was observed, which should be visible as intensity suppression in Figs. 5(c) and 5(d), meaning that TRS is not broken. In this sense, the Ho-doped films are comparable to the Gd-doped films,[28] but different than the Dy-doped films in which a gap has been observed,[27] despite the absence of magnetic long-range order.[26] Additional ARPES data are provided in the supplementary material.[30]

In conclusion, we presented a systematic study of the structural, magnetic, and electronic properties of high-quality MBE-grown $(Ho_xBi_{1-x})_2Te_3$ thin films. Ho was found to incorporate substitutionally on Bi sites of the rhombohedral crystal without the formation of secondary phases for Ho concentrations up to $x = 0.21$. The films were found to be paramagnetic down to the lowest probed temperature (2 K) with a doping concentration-independent effective magnetic moment of $\sim 5\,\mu_B$, determined by magnetometry. Evidence for possible antiferromagnetic ordering with a negative Weiss temperature was deduced from SQUID and XMCD measurements. Electronic bandstructure measurements revealed that the topological surface state remained intact upon Ho doping, further indicating the absence of TRS-breaking in the Ho-doped system. Despite the absence of TRS-breaking magnetic order Ho-doped films may still prove useful when proximity-coupled to a ferromagnet, for achieving the QAHE state.

This publication arises from research funded by the John Fell Oxford University Press (OUP) Research Fund and the Research Complex at Harwell is acknowledged for their hospitality. This work was supported by a DARPA MESO project (No. N66001-11-1-4105). S.E.H. was supported by the VPGE (Stanford University). L.C.M. and A.A.B. acknowledge partial financial support from EPSRC (UK) through a Doctoral Training Award. Diamond Light Source is acknowledged for beamtime on I10 (proposal SI10207). We thank A. Vailionis and Y. Huo for helpful discussions throughout the course of this work.

[1]C. Kane and E. Mele, Phys. Rev. Lett. **95**, 146802 (2005).
[2]B. A. Bernevig, T. L. Hughes, and S.-C. Zhang, Science **314**, 1757 (2006).
[3]Y. L. Chen, J.-H. Chu, J. G. Analytis, Z. K. Liu, K. Igarashi, H.-H. Kuo, X. L. Qi, S. K. Mo, R. G. Moore, D. H. Lu, M. Hashimoto, T. Sasagawa, S. C. Zhang, I. R. Fisher, Z. Hussain, and Z. X. Shen, Science **329**, 659 (2010).
[4]C. Niu, Y. Dai, M. Guo, W. Wei, Y. Ma, and B. Huang, Appl. Phys. Lett. **98**, 252502 (2011).
[5]C.-Z. Chang, J. Zhang, X. Feng, J. Shen, Z. Zhang, M. Guo, K. Li, Y. Ou, P. Wei, L.-L. Wang, Z.-Q. Ji, Y. Feng, S. Ji, X. Chen, J. Jia, X. Dai, Z. Fang, S.-C. Zhang, K. He, Y. Wang, L. Lu, X.-C. Ma, and Q.-K. Xue, Science **340**, 167 (2013).
[6]R. Li, J. Wang, X.-L. Qi, and S.-C. Zhang, Nat. Phys. **6**, 284 (2010).
[7]W.-K. Tse and A. H. MacDonald, Phys. Rev. Lett. **105**, 057401 (2010).
[8]X. Zhang and S.-C. Zhang, Proc. SPIE **8373**, 837309 (2012).
[9]A. R. Mellnik, J. S. Lee, A. Richardella, J. L. Grab, P. J. Mintun, M. H. Fischer, A. Vaezi, A. Manchon, E. A. Kim, N. Samarth, and D. C. Ralph, Nature **511**, 449 (2014).
[10]J. Wang, B. Lian, and S.-C. Zhang, Phys. Rev. Lett. **115**, 036805 (2015).
[11]Y. Xia, D. Qian, D. Hsieh, L. Wray, A. Pal, H. Lin, A. Bansil, D. Grauer, Y. S. Hor, R. J. Cava, and M. Z. Hasan, Nat. Phys. **5**, 398 (2009).
[12]J.-M. Zhang, W. Zhu, Y. Zhang, D. Xiao, and Y. Yao, Phys. Rev. Lett. **109**, 266405 (2012).
[13]V. Kulbachinskii, A. Kaminskii, K. Kindo, Y. Narumi, K. Suga, P. Lostak, and P. Svanda, Physica B **311**, 292 (2002).
[14]J. Choi, S. Choi, J. Choi, Y. Park, H. Park, H. Lee, B. Woo, and S. Cho, Phys. Status Solidi B **241**, 1541 (2004).
[15]J. W. G. Bos, M. Lee, E. Morosan, H. W. Zandbergen, W. L. Lee, N. P. Ong, and R. J. Cava, Phys. Rev. B **74**, 184429 (2006).
[16]Y. S. Hor, P. Roushan, H. Beidenkopf, J. Seo, D. Qu, J. G. Checkelsky, L. A. Wray, D. Hsieh, Y. Xia, S.-Y. Xu, D. Qian, M. Z. Hasan, N. P. Ong, A. Yazdani, and R. J. Cava, Phys. Rev. B **81**, 195203 (2010).

[17]M. Watson, L. Collins-McIntyre, A. Coldea, D. Prabhakaran, L. R. Shelford, S. C. Speller, T. Mousavi, C. Grovenor, Z. Salman, S. R. Giblin, G. van der Laan, and T. Hesjedal, New J. Phys. **15**, 103016 (2013).
[18]L. J. Collins-McIntyre, M. D. Watson, A. A. Baker, S. L. Zhang, A. I. Coldea, S. E. Harrison, A. Pushp, A. J. Kellock, S. S. P. Parkin, G. van der Laan, and T. Hesjedal, AIP Adv. **4**, 127136 (2014).
[19]R. Yu, W. Zhang, H.-J. Zhang, S.-C. Zhang, X. Dai, and Z. Fang, Science **329**, 61 (2010).
[20]P. P. J. Haazen, J. B. Laloe, T. J. Nummy, H. J. M. Swagten, P. Jarillo-Herrero, D. Heiman, and J. S. Moodera, Appl. Phys. Lett. **100**, 082404 (2012).
[21]L. J. Collins-McIntyre, S. E. Harrison, P. Schoenherr, N.-J. Steinke, C. J. Kinane, T. R. Charlton, D. Alba-Veneroa, A. Pushp, A. J. Kellock, S. S. P. Parkin, J. S. Harris, S. Langridge, G. van der Laan, and T. Hesjedal, EPL **107**, 57009 (2014).
[22]A. I. Figueroa, G. van der Laan, L. J. Collins-McIntyre, S.-L. Zhang, A. A. Baker, S. E. Harrison, P. Schoenherr, G. Cibin, and T. Hesjedal, Phys. Rev. B **90**, 134402 (2014).
[23]A. I. Figueroa, G. van der Laan, L. J. Collins-McIntyre, G. Cibin, A. J. Dent, and T. Hesjedal, J. Phys. Chem. C **119**, 17344 (2015).
[24]S. Li, S. Harrison, Y. Huo, A. Pushp, H. Yuan, B. Zhou, A. Kellock, S. Parkin, Y.-L. Chen, T. Hesjedal, and J. Harris, Appl. Phys. Lett. **102**, 242412 (2013).
[25]S. E. Harrison, L. J. Collins-McIntyre, S. Li, A. A. Baker, L. R. Shelford, Y. Huo, A. Pushp, S. S. P. Parkin, J. S. Harris, E. Arenholz, G. van der Laan, and T. Hesjedal, J. Appl. Phys. **115**, 023904 (2014).
[26]S. E. Harrison, L. J. Collins-McIntyre, S.-L. Zhang, A. A. Baker, A. I. Figueroa, A. J. Kellock, A. Pushp, S. S. P. Parkin, J. S. Harris, G. van der Laan, and T. Hesjedal, J. Phys.: Condens. Matter **27**, 245602 (2015).
[27]S. E. Harrison, L. J. Collins-McIntyre, P. Schönherr, A. Vailionis, V. Srot, P. A. van Aken, A. J. Kellock, A. Pushp, S. S. P. Parkin, J. S. Harris, B. Zhou, Y. L. Chen, and T. Hesjedal, Sci. Rep. **5**, 15767 (2015).
[28]S. Harrison, S. Li, Y. Huo, B. Zhou, Y.-L. Chen, and J. Harris, Appl. Phys. Lett. **102**, 171906 (2013).
[29]K. Virwani, S. E. Harrison, A. Pushp, T. Topuria, E. Delenia, P. Rice, A. Kellock, L. Collins-McIntyre, J. Harris, T. Hesjedal, and S. S. P. Parkin, Appl. Phys. Lett. **105**, 241605 (2014).
[30]See supplementary material at http://dx.doi.org/10.1063/1.4935235 for rocking curve analysis, reciprocal space maps, and bandstructure plots obtained at different photon energies.
[31]T. Holland and S. Redfern, Mineral. Mag. **61**, 65 (1997).
[32]A. Majid, A. Dar, and J. J. Zhu, J. Magn. Magn. Mater. **374**, 676 (2015).
[33]O. Zhong-Wen and R. Guang-Hui, Chin. Phys. B **22**, 097501 (2013).
[34]G. van der Laan, J. Phys.: Conf. Ser. **430**, 012127 (2013).
[35]G. van der Laan and A. I. Figueroa, Coord. Chem. Rev. **277–278**, 95 (2014).
[36]B. T. Thole, G. van der Laan, J. C. Fuggle, G. A. Sawatzky, R. C. Karnatak, and J. M. Esteva, Phys. Rev. B **32**, 5107 (1985).
[37]G. van der Laan, Lect. Notes Phys. **697**, 143 (2006).
[38]S. E. Harrison, B. Zhou, Y. Huo, A. Pushp, A. J. Kellock, S. S. P. Parkin, J. S. Harris, Y. Chen, and T. Hesjedal, Appl. Phys. Lett. **105**, 121608 (2014).
[39]Y.-L. Chen, J. G. Analytis, J. H. Chu, Z. K. Liu, S.-K. Mo, X. L. Qi, H. J. Zhang, D. H. Lu, X. Dai, Z. Fang, S. C. Zhang, I. R. Fisher, Z. Hussain, and Z.-X. Shen, Science **325**, 178 (2009).